Life Sciences 219 (2019) 20–30

Contents lists available at ScienceDirect

Life Sciences

journal homepage: www.elsevier.com/locate/lifescie

Anti-lung cancer activity and inhibitory mechanisms of a novel Calothrixin A derivative

Xiaohong Yang, Jiangsheng Gao, Jian Guo, Zimeng Zhao, Shao-Lin Zhang*, Yun He*

Chongqing Key Laboratory of Natural Product Synthesis and Drug Research, School of Pharmaceutical Sciences, Chongqing University, 55 South Daxuecheng Road, Chongqing 401331, PR China

ARTICLE INFO

Keywords:
Topo I inhibitor
Apoptosis
Cell cycle arrest
Autophagy
Migration

ABSTRACT

Aims: CAA45 is a calothrixin A (CAA) analogue with anti-cancer activity at nanomolar concentration. This study aimed to investigate the anti-lung cancer activity of CAA45 and explore its mechanisms of actions.

Main methods: CAA and CAA45 were synthesized and their inhibition on DNA topoisomerase I (Topo I) performed by evaluating the relaxation of supercoiled pBR322 plasmid DNA and their anti-lung cancer capacity determined by cytotoxic assays, cell migration, cell cycle, cell apoptosis, cell autophagy and related signaling proteins expression by western blot.

Key findings: CAA45 significantly inhibited human non-small cancer cell A549 and NCI-H1650 cells growth with IC_{50} values of 110 and 230 nM, respectively. In the A549 xenograft models, CAA45 displayed strong antitumor activities at a dose of 10 mg/kg. CAA45 inhibited Topo I activity and caused the cell cycle arrest at S phase, which also reduced A549 cell migration by inhibiting MMP-2 and MMP-9 expressions. Furthermore, CAA45 induced A549 cell apoptosis and autophagy. The apoptosis pathway was involved in the release of cytochrome *c* and caspase activation. CAA45 also inhibited Akt, activated JNK and up-regulated p53 signals in A549 cells, which may serve as a modulator to induce apoptosis and autophagy in cancer cells.

Significance: CAA45 exerted its anti-lung cancer effect via inhibition of Topo I, resulting in cell cycle arrest and cell migration, induction of mitochondria mediated cell apoptosis and autophagy via PI3K/Akt/JNK/p53 pathway. All these observations suggested that CAA45 could be a promising lead for anti-cancer drug discovery.

1. Introduction

Lung cancer is one of the leading causes of cancer-related mortality in China. The reported data showed that approximately 733,300 people were diagnosed with lung cancer and 610,200 died in China in 2015 [1]. The predominant form of this disease is non-small-cell lung cancer (NSCLC), with majority of patients diagnosed at advanced stages [2]. For many decades, cytotoxic drugs such as docetaxel, paclitaxel, platinum, gemcitabine and gefitinib were used for the treatment of NSCLC patients in clinic [3,4]. However, with the long-term use of the cytotoxic drugs, there is an increase in drug-resistance and genetic alterations of cancer cells over the last decade, which limit their usage [4]. To overcome these defects, researchers have been searching for novel scaffolds that function by binding to novel sites on clinically well validated targets which are conserved among cancer cells.

DNA topoisomerase I (Top I) is a well-known anticancer target, which is essential for topological manipulation of DNA during cellular events such as replication, transcription and repair. Calothrixin A (CAA) (Fig. 1), a novel indolo [3,2-j] phenanthridine alkaloid, isolated from cyanobacteria *Calothrix* in 1999 and was reported as a weak Top I inhibitor [5]. CAA showed potent anti-proliferative activities against a series of cancer cell lines including Hela cells, cultured (p53 proficient) CEM Leukemia cells and Jurkat cells, with IC_{50} values of 40, 200 and 1600 nM, respectively [5–7]. CAA was also reported to induce cell apoptosis in Jurkat cells. However, the exact mechanism how CAA induces cancer cell apoptosis remains unclear.

Our laboratory has been searching for novel anti-cancer agents [8–12], and we have completed the total synthesis of CAA [13]. A series of CAA analogues were synthesized and screened for their anticancer activities. Some of them displayed anti-cancer effects at nanomolar concentrations (data not shown). CAA45 (Fig. 1) is a CAA analogue with excellent anti-proliferative effect, especially against lung cancer cells. In the present study, we planned to get further insight on the anti-lung cancer activity of CAA45 and its potential effect mechanism.

* Corresponding authors.
E-mail addresses: zhangsl@cqu.edu.cn (S.-L. Zhang), yun.he@cqu.edu.cn (Y. He).

https://doi.org/10.1016/j.lfs.2018.12.052
Received 27 October 2018; Received in revised form 20 December 2018; Accepted 29 December 2018
Available online 31 December 2018

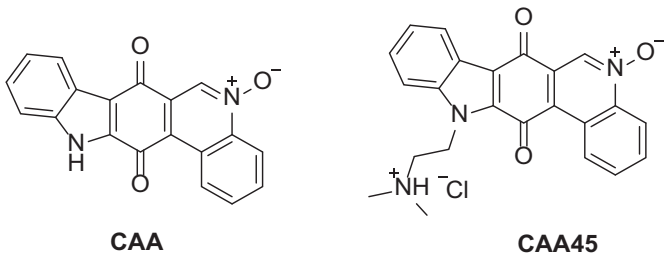

Fig. 1. Structures of CAA and CAA45.

2. Materials and methods

2.1. Chemicals and materials

CAA and CAA45 were synthesized in our lab [8]. Camptothecin (CPT) was obtained from Shanghai Macklin Biochemical Co. Ltd. and doxorubicin hydrochloride (DOX) was purchased from Shanghai Sangon Biotech Co. Ltd. Compounds were dissolved in DMSO at 10 mM as a stock solution, and diluted with culture medium. The maximum concentration of DMSO used in biological assays is < 0.1% (v/v) in the medium. For the in vivo drug administration, compound CAA45 was dissolved in sterilized ultra-pure water at 2 mg/mL, and the positive control drug CPT was dissolved in intralipid 20% at 1 mg/mL, the vehicle group was intralipid 20% without any drug. All the stock solutions were stored at −80 °C prior to use.

Cleaved caspase-3 (C-caspase-3), cleaved caspase-8 (C-caspase-8), cleaved caspase-9 (C-caspase-9), Bad, Bax, Bcl-2, Bcl-xl, phospho-Akt (*p*-Akt), phospho-JNK (*p*-JNK), p53 and LC3B antibodies were purchased from Cell Signaling Technology, Inc. (Danvers, MA, USA). Cytochrome C (Cyto-C), Cox IV, Akt, JNK, MMP-2 and MMP-9 were purchased from Abcam Biotechnology (Cambridge, MA, USA). The *β*-actin antibody and goat-anti-rabbit horseradish-peroxidase-conjugated (HRP) secondary antibodies were purchased from Beijing Biosynthesis Biotechnology Co., Ltd. (Beijing, China).

2.2. Cell cultures

Two NSCLC cell lines A549 and NCI-H1650, and two human normal cell lines BEAS-2B and L02 (human bronchial epithelial cell line BEAS-2B; human liver cell line L-02) were purchased from Shanghai Cell Bank of Chinese Academy of Sciences (Shanghai, China). A549 and BEAS-2B cells were maintained in DMEM (HyClone) medium supplemented with 10% fetal bovine serum (FBS), 1% penicillin and streptomycin. NCI-H1650 and L-02 cells were cultured in RPMI-1640 (HyClone) medium supplemented with 10% FBS, 1% penicillin and streptomycin. All the cells were cultured at 37 °C in a 5% CO_2 humidified atmosphere.

2.3. Cell viability assay

Cell viability upon treatment of the compounds was determined by using Cell Counting Kit-8 assay (Sangon Biotech, Shanghai, China) following the manufacturer's instructions. Cells were seeded in 96-well plates at density of 5×10^3 per well and were incubated for 72 h with either vehicle (DMSO) or desired concentrations of compounds at 37 °C in a 5% CO_2 incubator. Then, cells were incubated with CCK-8 solution for 1 h at 37 °C in a 5% CO_2 incubator. Finally, the absorbance at 450 nm was measured using a microplate reader (Bio-Rad Laboratories, Shanghai, USA). Cell viability was calculated as the ratio of the absorbance of the treated cells to the absorbance of the control groups. IC_{50} values were calculated by GraphPad Prism 6, which were the mean values derived from three independent experiments.

2.4. Colony formation assay

Colony formation assay was used to evaluate the anti-proliferative effect of CAA45 against A549 and NCI-H1650 cells as previously reported [14]. Varying cell numbers were seeded in 6-well plates and incubated at 37 °C for 24 h. Then the cells were treated with either DMSO or different concentrations of CAA45 (0.01, 0.03 and 0.06 μM) for 24 h, and then replaced by compound-free media for every 3 d. After 14 d cell plating, cell colonies were fixed with 4% paraformaldehyde for 15 min, and stained by 0.1% crystal violet for 30 min at room temperature. Colonies with over 100 cells were defined as positive.

2.5. DNA Top I inhibition assay

The inhibition of CAA45 on DNA Top I was performed indirectly by evaluating the relaxation of supercoiled pBR322 plasmid DNA. The experimental conditions were as previously reported [15]. Specifically, each reaction mixtures contained 2 μL 10× DNA Topo I buffer, 2 μL 0.1% BSA, 0.5 U Topo I protein, 0.25 μg of pBR322 plasmid DNA (Takara, Japan) and the test compound CAA45 (1, 5, and 10 μM) or positive control CPT (while the drug was omitted in control panel (panel 2) representing the capability of Topo I activity), then deionized water was used to complement the reaction volume to 20 μL. The reaction was performed at 37 °C in a water bath for 30 min and stopped by adding 1 μL 10% SDS and 3.5 μL 6× loading buffer. Finally, the reaction mixtures were separated by electrophoresis on a 1% agarose gel at 100 V for 40 min. The gels were stained with 0.5 mg/mL ethidium bromide for 15 min and visualized by using Molecular Imager FX (Biorad, Hemel Hempsted, UK).

2.6. Wound healing assay

A549 cells were seeded in 6-well plates at density of 1×10^6 cells/well. After reaching nearly confluence, a wound was created by using a p200 pipette tip in the middle area of confluent cells and then FBS free medium was used to remove the detached cells. Then cells were treated with either vehicle or CAA45 at the desired concentrations at 37 °C for 24 h. Images were taken by using phase-contrast microscopy (Olympus, IX51, Tokyo, Japan). The cell migration area was then calculated by ImageJ software (the formerly scratch area minus the final vacant area between cells). The ratio of migration area to the formerly scratched area indicates how many A549 cells migrate.

2.7. Transwell migration assay

Cells were suspended in serum-free DMEM and transferred on the top of transwell chambers (1×10^5 cells per Transwell) (Corning, New York, USA). DMEM with 10% fetal calf serum was placed in the lower chambers in the presence or absence of CAA45. After incubation for 24 h, the migrated cells in the bottom of the chamber were fixed by using 90% alcohol and stained with crystal violet staining solution (Beyotime, Jiangsu, China). Images were taken by using phase-contrast microscopy (Olympus, IX51, Tokyo, Japan). Five random fields per well were counted.

2.8. Apoptosis assay

Cells were seeded in 6-well plates at density of 1×10^5 cells/well and were allowed to grow overnight. Then the cells were treated with either DMSO or CAA45 (0.10, 0.20 and 0.30 μM) at 37 °C for 24 h. The cells were then trypsinized, repeatedly washed with cold PBS for three times, and centrifuged at 1200 rpm for 5 min- to pellet. Then the cells were resuspended to ~ 5×10^5 cells/mL in binding buffer (100 μL), stained with annexin-V-fluorescein isothiocyanate (FITC) (Sangon Biotech, Shanghai, China) and DAPI (Beyotime, Jiangsu, China) for 10 min at room temperature. Subsequently, the apoptotic cells were

immediately analyzed on a flow cytometer (Accuri C6, BD Biosciences). Cells undergoing early and late apoptosis were labeled by both annexin-V and DAPI, respectively.

2.9. Cell cycle assay

Cells (1×10^5 cells/well) were seeded in 6-well plates and treated with different concentrations of CAA45 (0.10, 0.20 and 0.30 μM) or 0.1% DMSO for 24 h at 37 °C. Then cells were harvested, washed with PBS and fixed with 70% precooled ethanol at −20 °C overnight. The fixed cells were washed with PBS and incubated with RNase A (Beyotime, Jiangsu, China) for 30 min at 37 °C. Finally, cells were stained with PI (Beyotime, Jiangsu, China) for 10 min at room temperature and analyzed on a flow cytometer (Accuri C6, BD Biosciences).

2.10. Monodansylcadaverine (MDC) incorporation assay

MDC incorporation assay was used to detect the formation of autophagic vacuoles. A549 cells were plated on coverslips in 24-well plates (2×10^4 cells/well) and treated with different concentrations of CAA45 (0.06, 0.12 and 0.25 μM) or DMSO (0.1%) or rapamycin (0.30 μM) for 12 h. Cells were then washed twice with PBS and incubated with fresh medium containing 0.05 mM MDC (Solarbio, Beijing, China) for 30 min at 37 °C. Then cells were washed four times with PBS and the autophagic vacuoles were detected on a confocal laser scanning microscopy (Leica TCS SP8, Solms, Germany).

2.11. Ad-mCherry-GFP-LC3B transfection

Cells (1×10^4 cells/well) were seeded on glass coverslips in 24-well plates and were allowed to grow overnight, then were transfected with Ad-mCherry-GFP-LC3B adenovirus (MOI value was 20) (Beyotime, Jiangsu, China) in 200 μL DMEM medium containing 10% FBS for 6 h. Subsequently cells were washed twice with PBS and treated with CAA45 (0.06, 0.12 and 0.25 μM) or rapamycin (0.30 μM) for 12 h. The treated cells were fixed with 4% paraformaldehyde for 20 min and washed three times with PBS. Finally, autophagy was observed using a confocal laser scanning microscopy (Leica TCS SP8, Solms, Germany).

2.12. Western blot

A549 cells were treated with desired concentrations of CAA45 for 24 h. Cells were then washed twice with ice-cold PBS and the total cellular protein was extracted by using western blot and IP cell lysis buffer kit (Beyotime, Jiangsu, China) following manufacturer's instructions. Protein concentrations were quantified using BCA Protein Assay Kit (Beyotime, Jiangsu, China) and then denaturized with SDS loading buffer at 100 °C for 8 min. Equal amounts of total protein (40 μg) was separated by 12% sodium dodecyl sulfate-polyacrylamide electrophoresis gels (SDS-PAGE) and then transferred onto polyvinylidene fluoride (PVDF) membrane, blocked with 5% fat-free dry milk/0.05% Tween 20 at room temperature for 2 h, breezed with desired primary monoclonal antibodies overnight, followed with horseradish peroxidase-conjugated goat anti-rabbit secondary antibody for 1 h. Finally, the immune reactive band was scanned in the enhanced chemiluminescence (ECL)-detecting reagents (Beyotime, Jiangsu, China) and optical density (OD) values were analyzed using Image J software.

2.13. Xenograft model

All animal studies were approved by the Laboratory Animal Welfare and Ethics Committee of the Third Military Medical University. Male BALB/c nude mice (5–7 weeks of age) were purchased from Chongqing Byrness Weil Biotechnology Co., Ltd. (Chongqing, China). Each animal was housed under standard conditions (21 ± 1 °C, 50–10% relative humidity, 12 h light/dark cycle) and had free access to food and water. A549 cells at 70–80% confluence were harvested with trypsin/EDTA, washed with PBS, and resuspended in serum-free DMEM medium. Cells (1×10^7) were inoculated in the right flank of each mouse subcutaneously. Within days after inoculation, the tumor bearing mice were randomly assigned into 4 treatment groups (3 mice/group) of vehicle, CPT (5 mg/kg), CAA45 (5 mg/kg) and CAA45 (10 mg/kg), and treated with specific doses of compound (s) by intramuscular injection twice a week. Tumor volume and body weight of each mouse were recorded twice a week. The tumor volume (mm^3) was calculated as follows: volume = (shortest diameter)^2 × (longest diameter) / 2. Mice were sacrificed by intraperitoneal injection of pentobarbital sodium (1%) in 42 days after medication. Then, tumor samples were harvested, formalin-fixed, subjected to hemotoxylin and eosin (H&E) staining for evaluating histological morphology under fluorescent microscopy.

2.14. Molecular docking

Molecular docking was performed using a Sybyl-X 2.0 software. The crystal structure of Topo I protein was downloaded from the Protein Data Bank (PDB ID: 1T8I). The crystal structure of Topo I was optimized with H added and charge added by AMBER7 FF99 method. The structures of small molecular database were subjected to the polar H adding and being energy optimized with a tripos force field and charged optimized with Gasteiger-Huckel method.

2.15. Statistical analysis

Data were expressed as the mean ± SEM, and $^*p < 0.05$ was considered statistically significant. Student's *t*-test was used to compare means between two groups, except tumor growth. Inhibition of tumor growth was analyzed by one-way ANOVA and LSD method. All analysis was performed by using the SPSS (V19.0, SPSS Inc., Chicago, IL, USA).

3. Results

3.1. CAA45 inhibited Topo I activity

Calothrixin A was reported as a weak Top I inhibitor. As a close analogue of Calothrixin A, CAA45 was expected to inhibit Top I. As shown in Fig. 2A, CAA45 caused a significant inhibition of Topo I activity in a concentration-dependent manner. Especially, the inhibitory activity of CAA45 at 10 μM outperformed CPT at the same concentration, suggesting that CAA45 possessed a stronger potency in Topo I inhibition as compared to the CPT. We then docked CAA45 into the Topo I binding pocket, and found that CAA45 formed direct hydrogen bonds interaction with Asn352 and Arg364 (Fig. 2B and C), which played crucial roles for Topo I's catalytical activity. These interactions could potentially explain the inhibitory activity of CAA45 on Topo I biological function.

3.2. CAA45 reduced cancer cell growths in vitro

To test the anti-proliferative activity of CAA45 on A549, NCI-H1650, BEAS-2B and L-02 cells were treated with various concentrations of CAA45 for 72 h and then the cell viability was evaluated using the CCK-8 kit. As shown in Fig. 3A, CAA45 exhibited promising anticancer activities on the two lung cancer cell lines A549 and NCI-H1650 with IC_{50} values of 110 and 230 nM, respectively, where DOX and CPT displayed weaker anti-proliferative activities with IC_{50} values of 460 and 320 nM against A549, and 480 and 320 nM against NCI-H1650, respectively. Interestingly, CAA45 exhibited superior selectivity indexes (SI) than CPT and DOX towards the A549 and NCI-H1650 cells over the two non-cancer cells tested (Fig. 3B). Especially, CAA45 showed a SI value of 8.52, outperformed CPT and DOX with SI values of 2.67 and 2.34 towards the A549 over L02, respectively. From Fig. 3C and D,

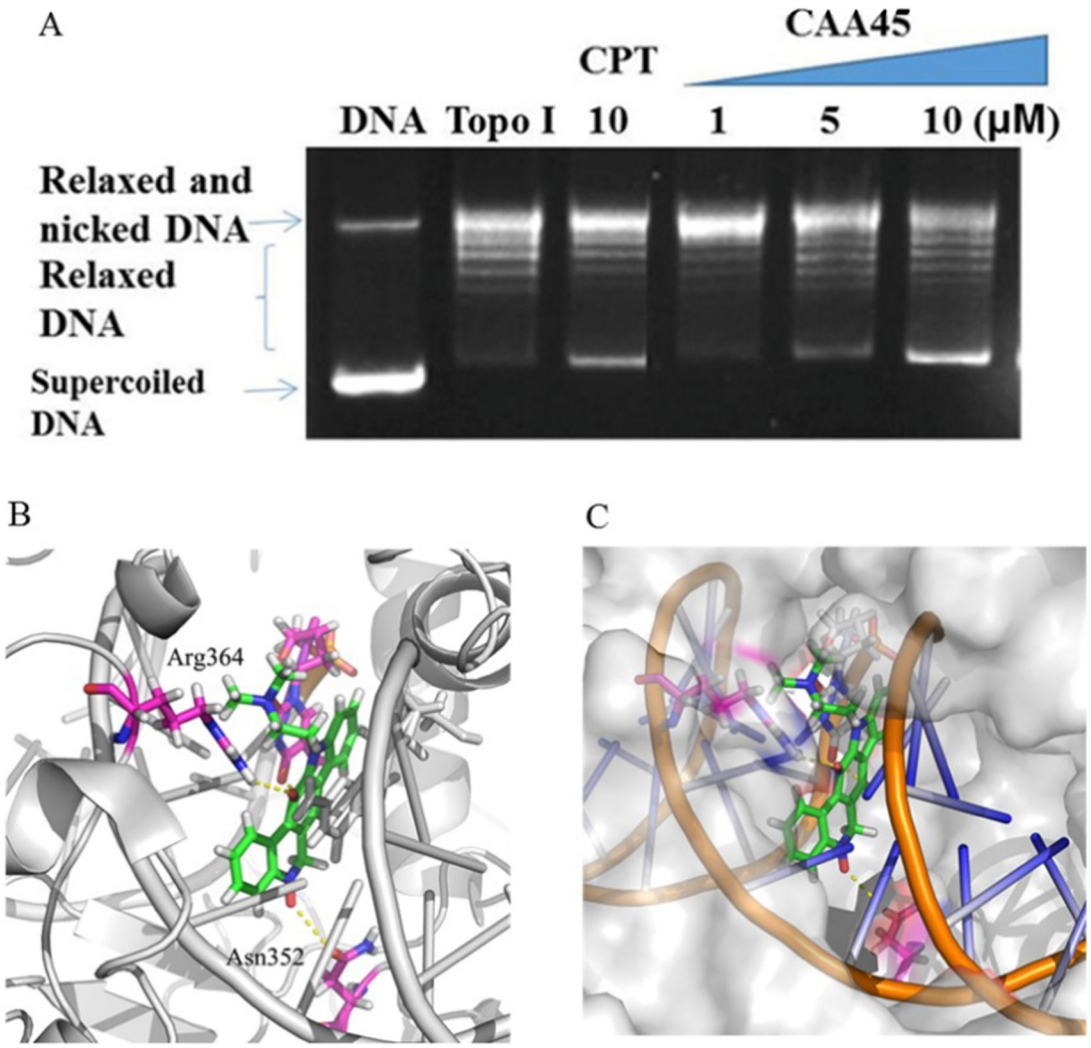

Fig. 2. (A) Effect of CAA45 on relaxation of supercoiled pBR322 DNA mediated by Topo I. Supercoiled DNA (lane DNA) incubated with Topo I in the absence (lane topo I) or in the presence of test compound at the indicated concentrations. CPT was used as a positive control. Lane 1, supercoiled plasmid DNA; lane 2, supercoiled plasmid DNA + Topo I; lane 3, supercoiled plasmid DNA + Topo I + CPT (10 μM); lanes 4–6, supercoiled plasmid DNA + Topo I + CAA45 (1, 5, and 10 μM). (B and C) Molecular docking of CAA45 with the Topo I (PDB code: 1T8I). Docking model of CAA45 in the binding pocket (B); stereo view of CAA45 in the binding pocket (C). Amino acid residues and compound CAA45 are shown as stick models, H-bonds are shown as yellow dashed lines. The 3D graphical presentations were drawn by PyMol. (For interpretation of the references to colour in this figure legend, the reader is referred to the web version of this article.)

CAA45 inhibited A549 and NCI-H1650 cell proliferation in concentration-dependent and time-dependent manners. In addition, CAA45 repressed the colony formation of A549 and NCI-H1650 cells. As shown in Fig. 3E and F, CAA45 clearly inhibited most of A549 and NCI-H1650 cell colony formation at 0.06 μM, and even at 0.01 μM, CAA45 was able to partially reduce its colony formation in both cancer cell lines. Moreover, A549 and NCI-H1650 cells formed fewer colonies with increment concentration of CAA45 in a dose response manner. All these results indicated that CAA45 exhibited a nanomolar anti-lung cancer activity, yet low toxicity against the normal human cell line.

3.3. CAA45 inhibited A549 cells migration

Since cell migration was observed in cell growth, we therefore investigated the effect of CAA45 on cell migration in A549 cells. The results of wound healing and transwell assays showed that A549 cell migration was significantly reduced ($p < 0.05$) after treating with CAA45 at 0.05, 0.10, and 0.15 μM as compared with the control group (Fig. 4A), suggesting that CAA45 strongly inhibits cancer cell migration. To understand if the reduced cancer cell migration is related to the protein matrix metalloproteinase-2 (MMP-2) and matrix metalloproteinase-9 (MMP-9), which degrade components of the extracellular matrix and thus play a pivotal role in cell migration during physiological and pathological processes, we next explored the effect of CAA45 on MMP-2 and MMP-9 expressions in A549 cells. As shown in Fig. 4B, the protein expression level of MMP-2 was significantly decreased after treating with CAA45 at 0.06, 0.10 and 0.15 μM. Similarly, MMP-9 protein expression was also significantly reduced with the treatment of CAA45 (0.15 μM). These results demonstrated that CAA45 inhibited A549 cells migration, partially ascribe to the reduction of the MMP-2 and MMP-9 expressions.

3.4. CAA45 induced A549 cell cycle arrest in S phase and apoptosis

To explore the mechanism of cancer cell cycle distribution after the treatment of CAA45, the A549 cells were treated with CAA45 at 0.10, 0.20, and 0.30 μM for 24 h, then cell cycle distribution was determined by a flow cytometer. As shown in Fig. 5A, upon treating with CAA45 at 0.10, 0.20, and 0.30 μM, the ratios of cells in the S phase increased to 26.87%, 34.40% and 42.36%, respectively.

To explore the mechanism of cancer cells death, CAA45 was used to induce A549 cells apoptosis, which was then examined with Annexin V-

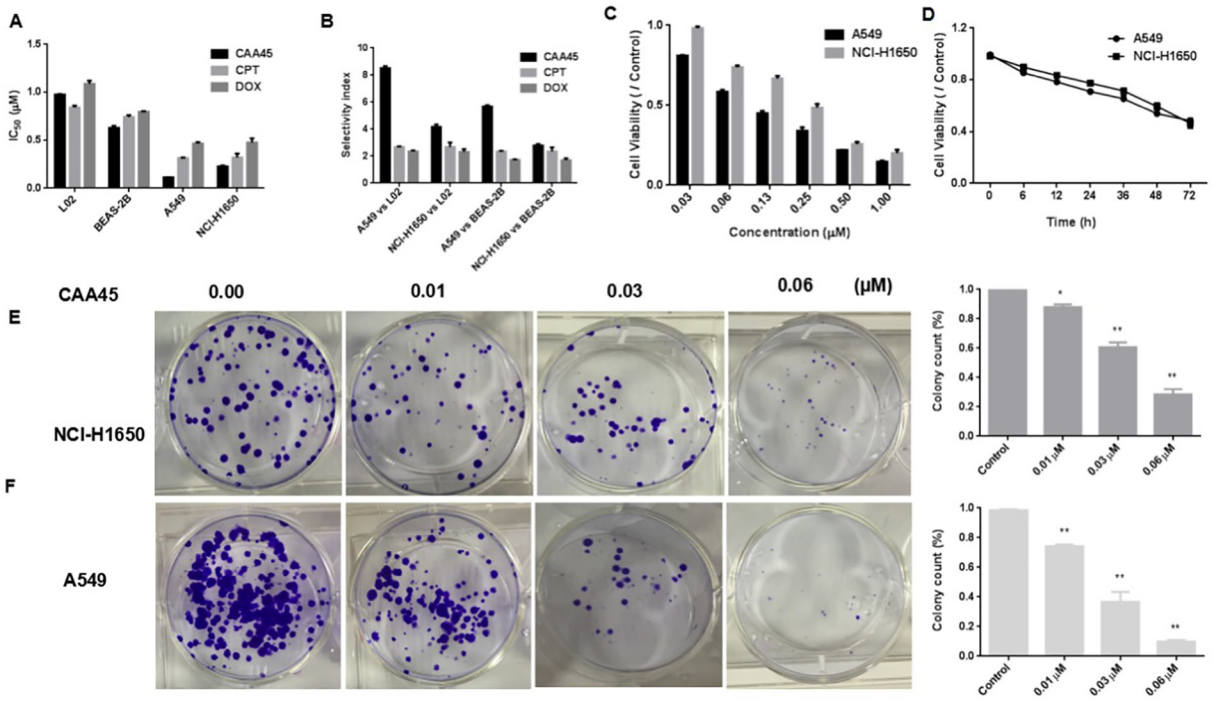

Fig. 3. Response of lung cancer and non-cancer cell lines to CAA45. (A) Cytotoxicity of CAA45 against lung cancer and non-cancer cell lines. Data are the mean ± SEM for 3 independent experiments. (B) The selectivity index was calculated from the IC_{50} values of non-cancer cell lines L02 or BEAS-2B dividing by the IC_{50} values of either A549 or NCI-H1650 cells. Selectivity index > 1 denotes preferential activity against cancer as compared to non-cancer cells, whereas the value < 1 denotes equivalent or reduced activity against cancer cells as compared to non-cancer cells. (C) Full dose responses of CAA45 inhibiting A549 and NCI-H1650 cell proliferation. (D) CAA45 time dependently inhibited A549 and NCI-H1650 cell growth. (E, F) CAA45 inhibited A549 and NCI-H1650 cell colony formations.

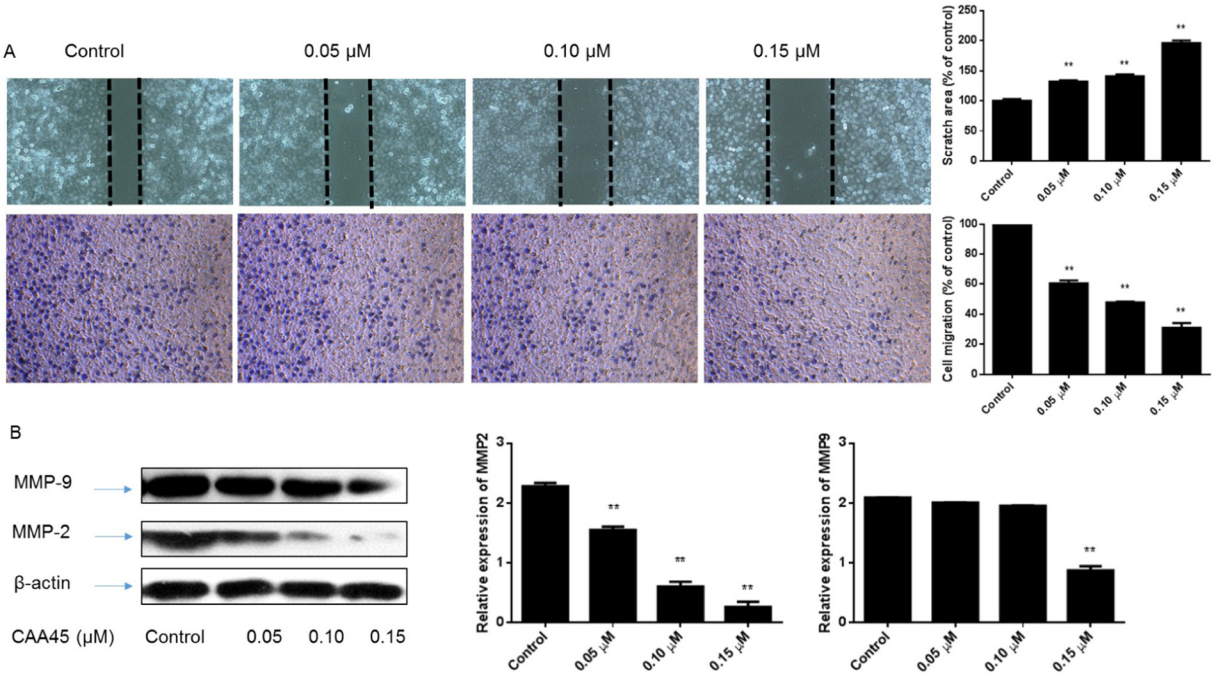

Fig. 4. CAA45 inhibited A549 cells migration. A549 cells were treated with DMSO or CAA45 (0.05, 0.10, and 0.15 μM) for 24 h. (A) The upper photo showed the closure of A549 cells after being scratched (×100) for 24 h, while the below showed the crystal violet stained A549 cells, which migrated to lower chamber after transwell (×100) for 24 h; (B) Western blot analysis of MMP-2 and MMP-9 expression in A549 cells. Bar graph represents mean ± SEM of the MMP-2 and MMP-9 expression level, which were derived from the optical density (OD) of immune reactive band analyzing by image J software. Each determination was done at least in triplicate. * = $p < 0.05$ vs control, ** = $p < 0.01$ vs control. (For interpretation of the references to colour in this figure legend, the reader is referred to the web version of this article.)

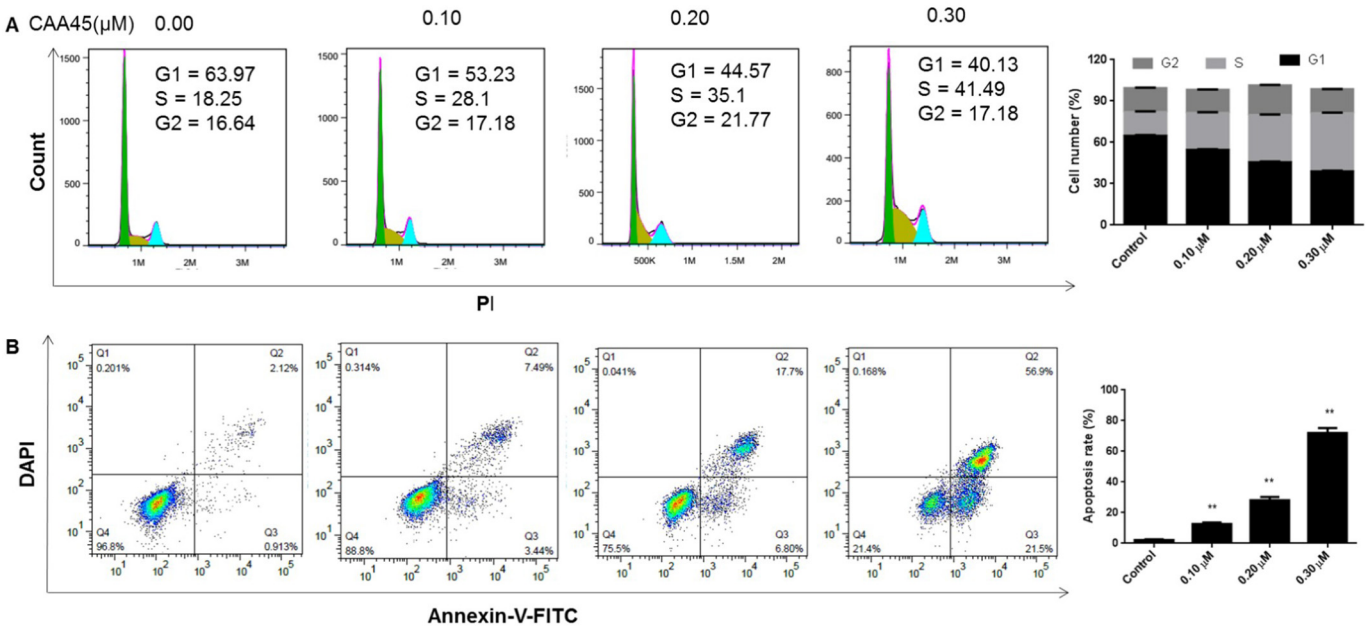

Fig. 5. Induction of cell cycle arrest and apoptosis by CAA45 treatment. A549 cells were treated with DMSO or CAA45 at different concentrations for 24 h. (A) Cells were stained with PI and cell cycle distribution was analyzed by using a flow cytometer. (B) For apoptosis, cells were stained with Annexin V-FITC/DAPI and analyzed using a flow cytometer. The values represent the mean ± SEM for three separate experiments. * = $p < 0.05$ vs control, ** = $p < 0.01$ vs control.

FITC/DAPI FACS assay. As shown in Fig. 5B, the percentages of apoptotic population in A549 cells treated with CAA45 at 0.10, 0.20 and 0.30 μM for 24 h were 12.68%, 28.23% and 71.94%, respectively, in a concentration dependent manner.

Furthermore, protein immunoblotting data showed that the expression level of cytochrome *c* in cell cytoplasm was increased gradually by treating with increased concentrations of CAA45 (0.06, 0.12, 0.25 μM) ($p < 0.05$ or $p < 0.01$), while significantly decreased ($p < 0.01$) in mitochondria (Fig. 6). These results indicated that CAA45 promoted the release of cytochrome *c* from mitochondria into cell cytoplasm.

To further explore the mechanism by which CAA45 induced apoptosis, we determined the protein expressions of C-caspase-3, C-caspase-8, C-caspase-9, Bad, Bax, Bcl-2 and Bcl-xl in A549 cells. As shown in Figs. 7 and 8, exposure of A549 cells to CAA45 (0.06, 0.12, and 0.25 μM) led to a significant increase in levels of C-caspase-3 ($p < 0.01$), C-caspase-8 ($p < 0.01$), C-caspase-9 ($p < 0.01$), Bad ($p < 0.01$) and Bax ($p < 0.01$), whereas the Bcl-2 expression was obviously decreased ($p < 0.01$). These data suggested that the pro-apoptotic effect of CAA45 was due to the mitochondria-mediated apoptosis.

3.5. CAA45 induced autophagy in A549 cells

MDC incorporation assay is an autofluorescent substance which selectively accumulates in acidic vesicular organelles (AVOs), and therefore is used as a marker for autophagy. As shown in Fig. 9A, after treatment with CAA45, the number of autophagic vacuoles was

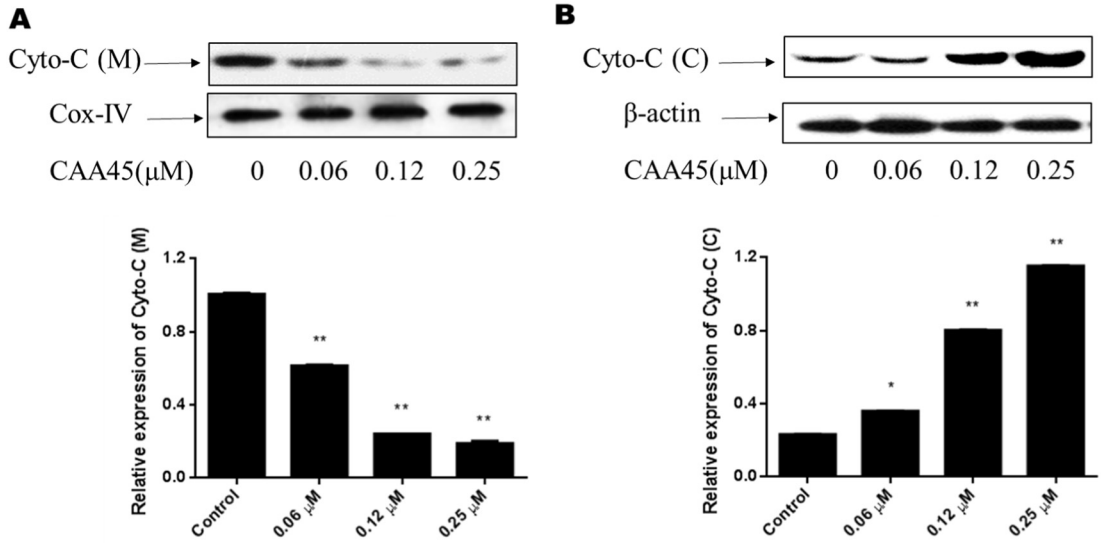

Fig. 6. CAA45 induced the release of cytochrome *c*. A549 cells were treated with DMSO or CAA45 (0.06, 0.12, 0.25 μM) for 24 h. The mitochondria and cytosolic factions were isolated. Cytochrome c in mitochondria (Cyto-C (M)) (A) and cytochrome *c* in cytoplasm (Cyto-C (C)) (B) expressions were detected by western blot. The values obtained represent the mean ± SEM for three separate experiments. * = $p < 0.05$ vs control, ** = $p < 0.01$ vs control.

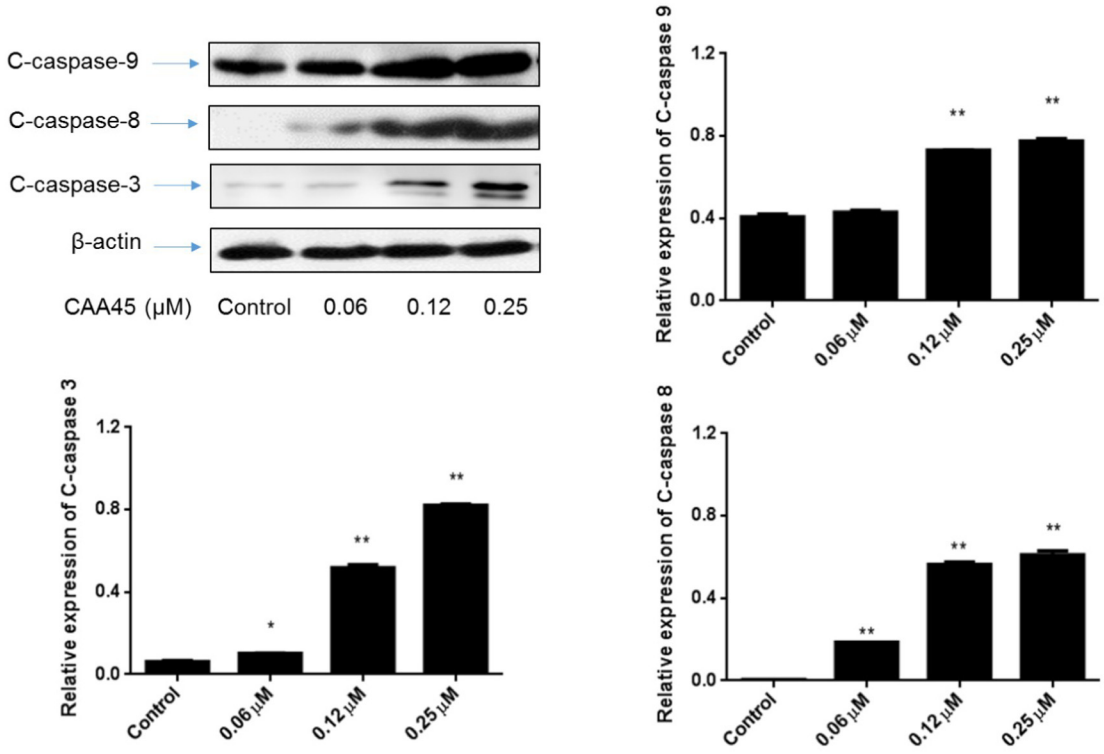

Fig. 7. CAA45 induced caspase activation in A549 cells. Cells were treated with DMSO or CAA45 (0.06, 0.12, and 0.25 μM) for 24 h. C-caspase 3, C-caspase 8 and C-caspase 9 expressions were detected by western blot. The values obtained represent the mean ± SEM for three separate experiments. * = $p < 0.05$ vs control, ** = $p < 0.01$ vs control.

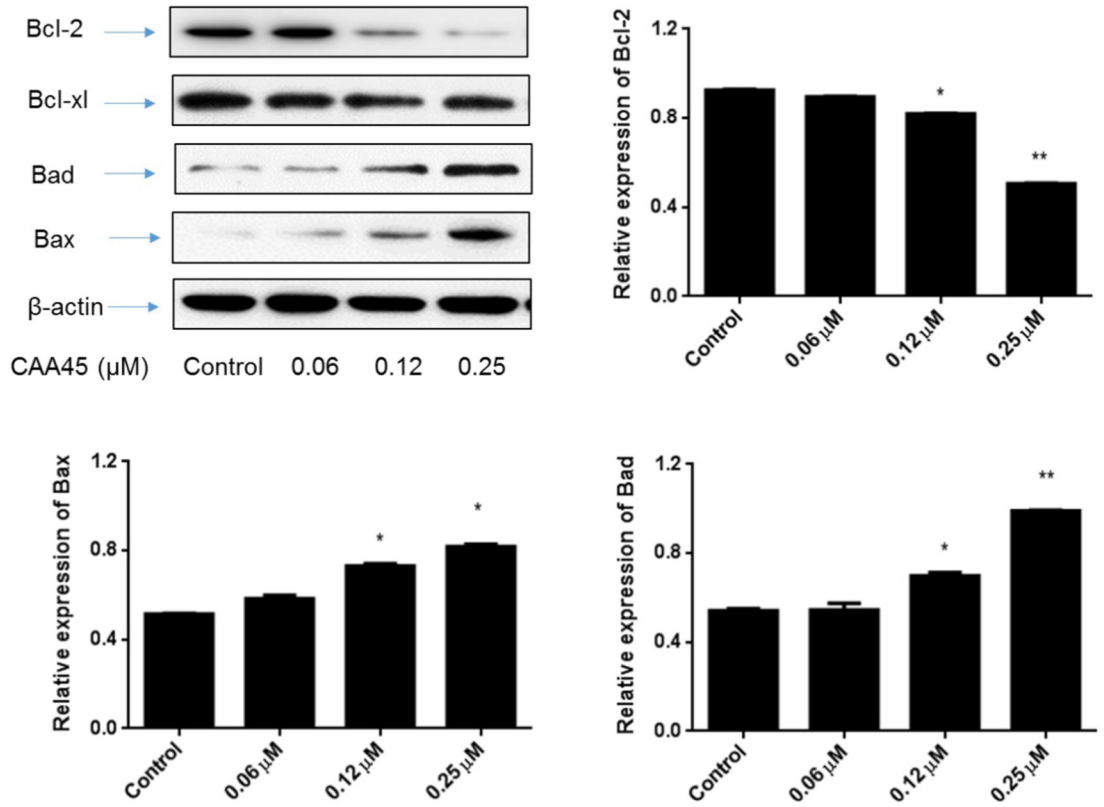

Fig. 8. CAA45 regulated Bcl-2 family protein expressions in A549 cells. Cells were treated with DMSO or CAA45 (0.06, 0.12, and 0.25 μM) for 24 h. Bcl-2, Bcl-xl, Bad and Bax expressions were detected by western blot. The values obtained represent the mean ± SEM for three separate experiments. * = $p < 0.05$ vs control, ** = $p < 0.01$ vs control.

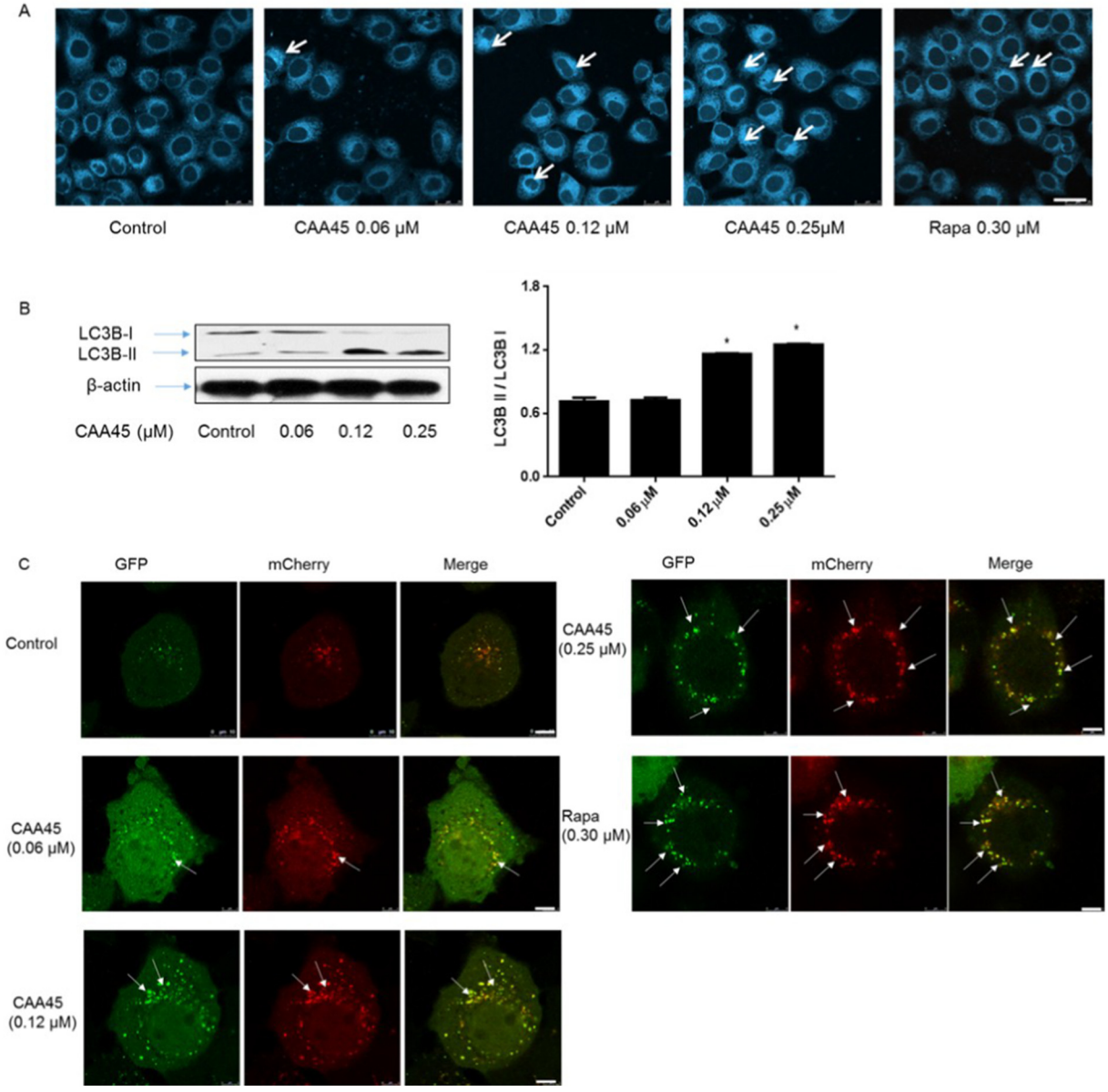

Fig. 9. Effect of CAA45 on autophagy in A549 cell. (A) Cells were plated on coverslips in 24-well plates, treated with CAA45 (0, 0.06, 0.12, 0.25 μM) or Rapa (0.30 μM) for 12 h, then stained with 0.05 mM MDC for 30 min at 37 °C. After washing with PBS, the stained A549 cells were immediately examined by Leica TCS Sp8 confocal microscope. Organelles stained with bright blue fluorescence indicate the autophagic vacuoles. Scale bar: 25 μm. (B) After treatment with CAA45 (0, 0.06, 0.12, 0.25 μM) for 12 h, cell lysates were prepared for western blot. The autophagy marker protein LC3-B were detected as described in the Materials and methods section. (C) A549 cells were transfected for 6 h with Ad-mCherry-GFP-LC3B adenovirus at an MOI of 20 at 37 °C, then treated with 1% DMSO, CAA45 or Rapa for 12 h. The treated cells were fixed to be available for microscopy. The GFP/mCherry images were acquired using Leica TCS Sp8 confocal microscope. Scale bar: 5 μm. Rapa: rapamycin. (For interpretation of the references to colour in this figure legend, the reader is referred to the web version of this article.)

increased in A549 cells, suggesting that CAA45 induced autophagy in A549 cells. As expected, rapamycin also increased the number of autophagic vacuoles under the same conditions.

To further evaluate the influence of CAA45 on autophagy, we transfected A549 cells with Ad-mCherry-GFP-LC3B adenovirus. As shown in Fig. 9C, only signals of GFP and mCherry protein which represent diffuse LC3 protein were found in the cytoplasm before treatment of CAA45. After treatment with CAA45 at 0.06, 0.12, and 0.25 μM for 12 h, the mCherry and GFP dot signals significantly increased in A549 cells, suggesting that CAA45 induced autophagic vacuole formation.

Finally, we determined the effect of CAA45 on the expression of LC3B, an autophagy marker protein. As shown in Fig. 9B, after treatment with CAA45 for 12 h, the conversion of LC3B I to II increased in a concentration-dependent manner, further demonstrating the autophagy-inducing activity of CAA45.

3.6. CAA45 induced Akt inactivation, JNK activation and up-regulation of p53 in A549 cells

It has been reported that the PI3K/Akt pathway, MAPK (JNK) signaling and p53 play important roles in cell proliferation, survival, apoptosis and autophagy. However, the relationship between these signaling pathways and the effect of CAA45 on proliferation, migration and autophagy of lung cancer cells has not yet been reported. Our study aimed to explore the potential effect mechanisms. As shown in Fig. 10A, the expressions of p-AKT in A549 cells after treating with CAA45 were significantly reduced ($p < 0.01$). In addition, the phosphorylation of

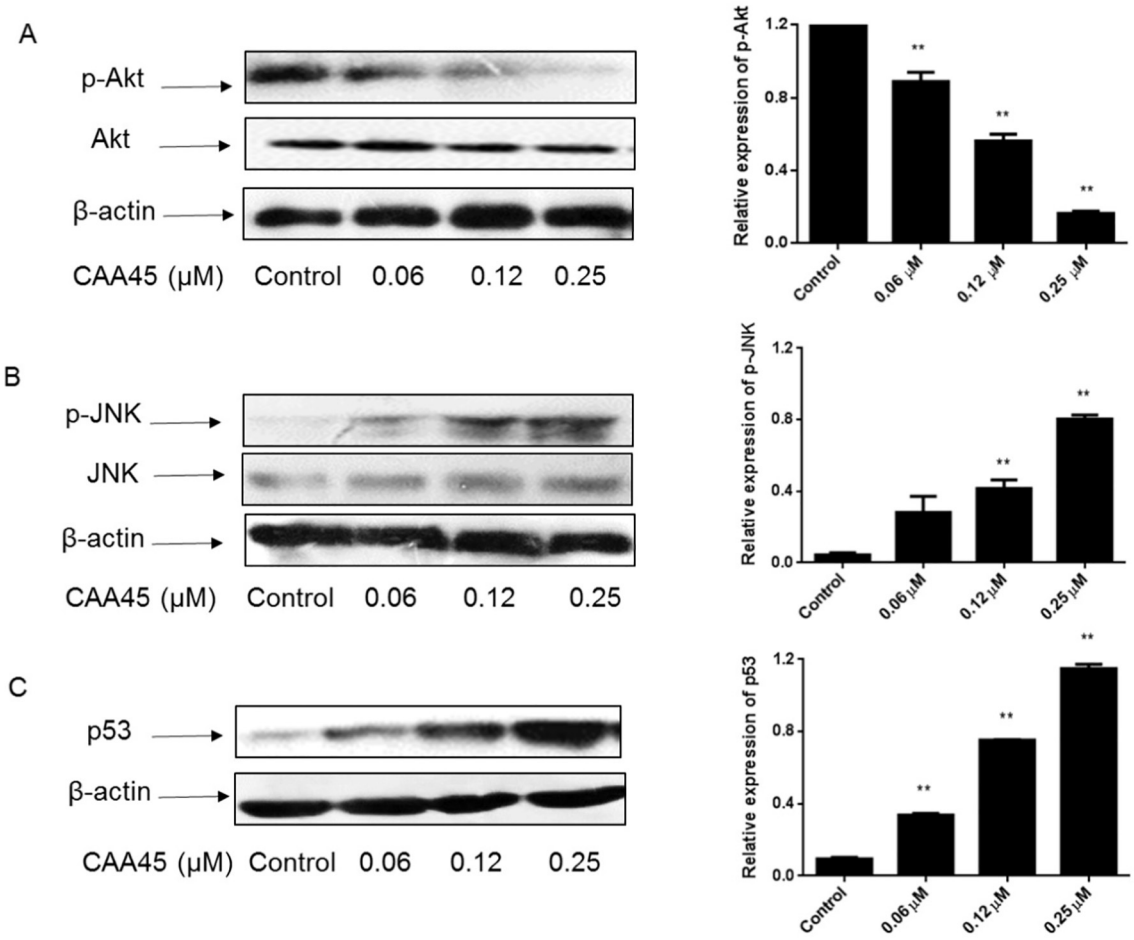

Fig. 10. CAA45 induced Akt inactivation, JNK activation and up-regulation of p53 expression in A549 cells. Cells were treated with DMSO or CAA45 for 24 h. Phosphorylated Akt (p-Akt), Akt, phosphorylated JNK (p-JNK), and JNK, p53 expressions were detected by western blot. The values obtained represent the mean ± SEM for three separate experiments. * = $p < 0.05$ vs control, ** = $p < 0.01$ vs control.

JNK increased by treating with CAA45 ($p < 0.01$), as compared to the control group (Fig. 10B). Furthermore, CAA45 significantly increased p53 protein expression in A549 cells (Fig. 10C).

3.7. CAA45 inhibited tumor growth in vivo

The in vivo antitumor activities of CAA45 were evaluated in a nude mouse xenograft model. As shown in Fig. 11A, CAA45 led to a significant reduction in tumor growth as compared to the untreated controls for 42 days following drug exposure ($p < 0.01$). To evaluate whether CAA45 treatment might result in morphological changes in A549 cells in vivo, excised tumor samples were sectioned and stained with H&E. H&E staining of sections of the tumors from mice treated with CAA45 exhibited significant changes in morphology, with signs of apoptotic cells (Fig. 11C). However, compared to the vehicle group, slight body weight gain (Fig. 11B) was observed among treat groups. The slow body weight gain suggested that CAA45 might have some toxicity, similar to the control drug CPT.

4. Discussion

We synthesized a potent CAA analogue CAA45, fully evaluated its anti-lung cancer activity, and explored its mechanism of action. This study is the first report that CAA45 inhibits human non-small cancer cell growth in vitro and in vivo. CAA45, a Topo I inhibitor, is found to cause cell cycle arrest in S phase, induce cell apoptosis and autophagy, and inhibit cell migration in A549 cells. Furthermore, we found that the pro-apoptotic effect of CAA45 was regulated by mitochondria mediated apoptosis pathway. Both CAA45 induced apoptosis and autophagy were regulated by Akt/JNK/p53 signaling pathway.

Topo I is a promising target for developing anti-cancer drugs. Our data demonstrated that CAA45 strongly inhibited Topo I activity at 10 μM, outperforming CPT under the same experimental conditions. Furthermore, CAA45 induced cell cycle arrest in the S phase in A549 cells, indicating intracellular DNA damage. Based on the above observations, we could conclude that inhibition of Topo I enzyme by CAA45 contributed to the DNA damage, resulting in cell cycle arrest at S phase and inhibition of cell proliferation.

It is common that lung cancer patients have metastasis, which leads to treatment failures [4,16,17]. Metastatic lung cancer is characterized by uncontrolled cell growth in tissues of the lung, which can spread beyond the lung into nearby tissues or other parts of the body by the process of metastasis [18]. To evaluate the inhibition ability of CAA45 on the migration of A549 cells, we performed wound healing and transwell assays. Our data demonstrated that CAA45 significantly inhibited A549 cells migration by reducing MMP-2 and MMP-9 expressions, which might lead to inhibition of cell proliferation.

CAA was reported to induce cell apoptosis [19], but their mediated signaling pathways remained unknown. In our study, we found that CAA analogue CAA45 induced A549 cell apoptosis in a concentration-dependent manner. Our results provided more detailed information on the molecular mechanisms by which CAA45 induces apoptosis in A549 cells (i.e. by enhanced cytochrome *c* release, caspase-3, -8 and -9 cleavage activation, increased expression of Bax and Bad, and

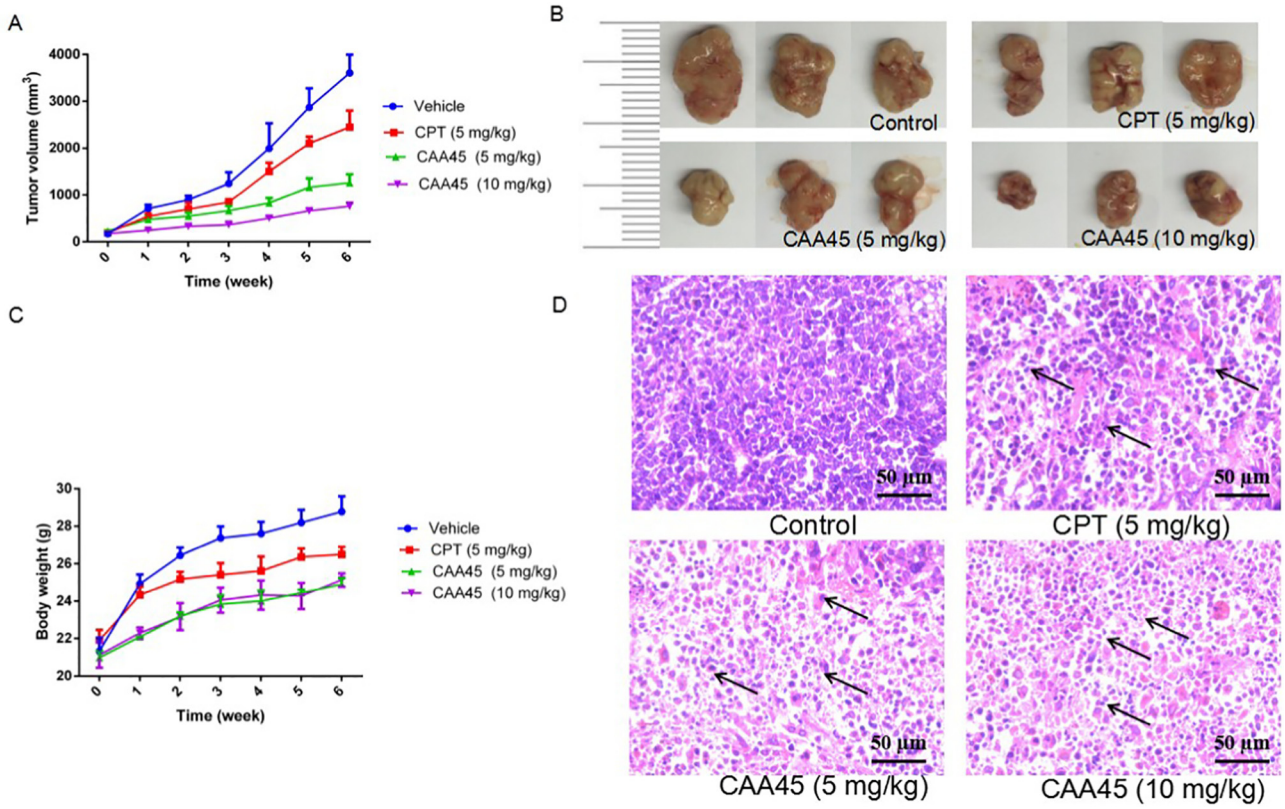

Fig. 11. CAA45 significantly inhibited tumor growth in A549 mouse xenograft model. Male BALB/c nude mice (5–7 weeks of age) were inoculated with A549 cells. After tumor inoculation, the mice were randomly assigned into 4 treatment groups (3 mice/group) of vehicle, CPT (5 mg/kg), CAA45 (5 mg/kg) and CAA45 (10 mg/kg) was administered by intramuscular injection twice a week. (A) Average tumor volume and (B) body weight changes of mice during 6 weeks of exposure. Error bars represent means ± SEM for a total of 3 samples. After the 42-day drug administration, tumor tissues of each samples were harvested, photographed (C), sectioned and subjected to H&E staining (D) for evaluating histological morphology under fluorescent microscopy (40×).

decreased expression of Bcl-2), which is clearly related to the mitochondrial mediated apoptosis pathway [20,21]. Up-regulated Bad and Bax and down-regulated Bcl-2 expressions led to the release of cytochrome *c* from mitochondria to the cytoplasm, subsequently activating the caspase-3, caspase-8 and caspase-9 signal pathways. Caspase-3 activation is recognized as a biomarker for cells undergoing apoptosis [22,23]. Therefore, CAA45 induced apoptosis occurs via a mitochondrial-mediated pathway in A549 cells.

Apoptosis and autophagy have coordinated and cooperative interactions to promote cell death under certain circumstances, and type I apoptosis and type II autophagic cell death collaborate to kill cells [24,25]. Our study has shown that CAA45 not only induced apoptosis but also enhanced autophagy in A549 cells, suggesting that inhibition of lung cancer cell proliferation by CAA45 was promoted by both autophagy and apoptosis. Furthermore, treatment of cells with CAA45 resulted in inactivation of JNK and Akt, and up-regulation of p53. It has been reported that the PI3K/Akt pathway, MAPK (JNK) signaling and p53 play important roles in cell proliferation, apoptosis and autophagy [26–29]. It is possible that CAA45 induced apoptosis and autophagy was medicated by the PI3K/Akt/JNK/p53 pathway.

To further demonstrate antitumor activity of CAA45, the tumor xenograft model bearing A549 cancer cell in BALB/c nude mouse was established and evaluated its anticancer activity in vivo. CAA45 at 5 or 10 mg/kg was able to reduce the tumor growth relative to the vehicle group. However, a slight body weight gain was observed among treat groups including the CPT treatment group as compared to the vehicle group, which may due to the fact that CAA45 may have some toxicity, similar as CPT. Further studies will be conducted to disclose the causes of the slight body weight gain.

5. Conclusions

In conclusion, the present study indicated that CAA45 potently inhibited lung cancer proliferation with good selectivity over normal cells. CAA45 exerted its anticancer effect by multiple mechanisms involving (i) inhibition of DNA Topo I activity, leading to DNA damage which results in cell cycle arrest at S phase; (ii) inhibition of cell migration; (iii) induction of mitochondria mediated apoptosis and (iv) autophagy via PI3K/Akt/JNK/p53 pathway. Therefore, CAA45 could be considered as a promising lead compound targeting multiple important pathways in cancer biology. Further studies to understand the molecular interactions and optimize the pharmaceutical properties of CAA45 are ongoing in our laboratory and the results shall be reported in due course.

Conflict of interest

The authors declare no conflict of interest.

Acknowledgements

This work was supported by the National Natural Science Foundation of China (No. 21572027, 21807008). We thank Yanfei Qiu and Hongmei Tian for technical assistance with animal studies.

Competing interests

The authors declare that no competing interests exist.

References

[1] P. Wang, J. Zou, J. Wu, C. Zhang, C. Ma, J. Yu, et al., Clinical profiles and trend analysis of newly diagnosed lung cancer in a tertiary care hospital of East China during 2011–2015, J. Thorac. Dis. 9 (2017) 1973–1979.

[2] L. Zhang, SC17.02 lung cancer in China: challenges and perspectives, J. Thorac. Oncol. 12 (2017) S113–S114.

[3] F.R. Hirsch, K. Suda, J. Wiens, P.A. Bunn, New and emerging targeted treatments in advanced non-small-cell lung cancer, Lancet 388 (2016) 1012–1024.

[4] F.R. Hirsch, G.V. Scagliotti, J.L. Mulshine, R. Kwon, W.J. Curran, Y.-L. Wu, et al., Lung cancer: current therapies and new targeted treatments, Lancet 389 (2017) 299–311.

[5] R.W. Rickards, J.M. Rothschild, A.C. Willis, N.M. de Chazal, J. Kirk, K. Kirk, et al., Calothrixins A and B, novel pentacyclic metabolites from Calothrix cyanobacteria with potent activity against malaria parasites and human cancer cells, Tetrahedron 55 (1999) 13513–13520.

[6] P.H. Bernardo, C.L.L. Chai, G.A. Heath, P.J. Mahon, G.D. Smith, P. Waring, et al., Synthesis, electrochemistry, and bioactivity of the cyanobacterial calothrixins and related quinones, J. Med. Chem. 47 (2004) 4958–4963.

[7] Q.A. Khan, J. Lu, S.M. Hecht, Calothrixins, a new class of human DNA topoisomerase I poisons, J. Nat. Prod. 72 (2009) 438–442.

[8] Y. Addepalli, X. Yang, M. Zhou, D.P. Reddy, S.-L. Zhang, Z. Wang, et al., Synthesis and anticancer activity evaluation of novel azacalix[2]arene[2]pyrimidines, Eur. J. Med. Chem. 151 (2018) 214–225.

[9] N. Zhang, Z. Yu, X. Yang, Y. Zhou, Q. Tang, P. Hu, et al., Difuran-substituted quinoxalines as a novel class of PI3Kα H1047R mutant inhibitors: synthesis, biological evaluation and structure-activity relationship, Eur. J. Med. Chem. 157 (2018) 37–49.

[10] N. Zhang, Z. Yu, X. Yang, Y. Zhou, J. Wang, S.-L. Zhang, et al., Synthesis, biological evaluation and structure-activity relationship of a novel class of PI3Kα H1047R mutant inhibitors, Eur. J. Med. Chem. 158 (2018) 707–719.

[11] N. Zhang, Z. Yu, X. Yang, P. Hu, Y. He, Synthesis of novel ring-contracted artemisinin dimers with potent anticancer activities, Eur. J. Med. Chem. 150 (2018) 829–840.

[12] B. Xu, Z. Yu, S. Xiang, Y. Li, S.-L. Zhang, Y. He, Rational design of mitochondria-targeted pyruvate dehydrogenase kinase 1 inhibitors with improved selectivity and antiproliferative activity, Eur. J. Med. Chem. 155 (2018) 275–284.

[13] J. Guo, I.C. Kiran, J. Gao, R.S. Reddy, Y. He, Total synthesis of calothrixins and their analogues via formal [3 + 2] cycloaddition of arynes and 2-aminophenanthridinedione, Tetrahedron Lett. 57 (2016) 3481–3484.

[14] Z. Yang, X. Hu, S. Zhang, W. Zhang, K.Y. Tam, Pharmacological synergism of 2,2-dichloroacetophenone and EGFR-TKi to overcome TKi-induced resistance in NSCLC cells, Eur. J. Pharmacol. 815 (2017) 80–87.

[15] G. Dong, C. Sheng, S. Wang, Z. Miao, J. Yao, W. Zhang, Selection of evodiamine as a novel topoisomerase I inhibitor by structure-based virtual screening and hit optimization of evodiamine derivatives as antitumor agents, J. Med. Chem. 53 (2010) 7521–7531.

[16] A.F. Chambers, A.C. Groom, I.C. MacDonald, Metastasis: dissemination and growth of cancer cells in metastatic sites, Nat. Rev. Cancer 2 (2002) 563–572.

[17] J.R. Molina, P. Yang, S.D. Cassivi, S.E. Schild, A.A. Adjei, Non-small cell lung cancer: epidemiology, risk factors, treatment, and survivorship, Mayo Clin. Proc. 83 (2008) 584–594.

[18] W.D. Travis, Pathology of lung cancer, Clin. Chest Med. 32 (2011) 669–692.

[19] X. Chen, G.D. Smith, P. Waring, Human cancer cell (Jurkat) killing by the cyanobacterial metabolite calothrixin A, J. Appl. Phycol. 15 (2003) 269–277.

[20] S. Xiong, T. Mu, G. Wang, X. Jiang, Mitochondria-mediated apoptosis in mammals, Protein Cell 5 (2014) 737–749.

[21] W. Peng, C. Hu, Z. Shu, T. Han, L. Qin, C. Zheng, Antitumor activity of tatariside F isolated from roots of *Fagopyrum tataricum* (L.) Gaertn against H22 hepatocellular carcinoma via up-regulation of p53, Phytomedicine 22 (2015) 730–736.

[22] K.-M. Debatin, Apoptosis pathways in cancer and cancer therapy, Cancer Immunol. Immunother. 53 (2004) 153–159.

[23] H. Okada, T.W. Mak, Pathways of apoptotic and non-apoptotic death in tumour cells, Nat. Rev. Cancer 4 (2004) 592–603.

[24] B. Levine, Cell biology: autophagy and cancer, Nature 446 (2007) 745–747.

[25] B. Levine, J. Yuan, Autophagy in cell death: an innocent convict? J. Clin. Invest. 115 (2005) 2679–2688.

[26] L. Ouyang, Z. Shi, S. Zhao, F.T. Wang, T.T. Zhou, B. Liu, et al., Programmed cell death pathways in cancer: a review of apoptosis, autophagy and programmed necrosis, Cell Prolif. 45 (2012) 487–498.

[27] J. Luo, B.D. Manning, L.C. Cantley, Targeting the PI3K-Akt pathway in human cancer: rationale and promise, Cancer Cell 4 (2003) 257–262.

[28] D.N. Dhanasekaran, E.P. Reddy, JNK signaling in apoptosis, Oncogene 27 (2008) 6245–6251.

[29] C.A. Iacobuzio-Donahue, J.M. Herman, Autophagy, p53, and pancreatic cancer, Cell Prolif. 370 (2014) 1352–1353.